



ORIGINAL ARTICLE

Numerical investigation of thermal performance of heat sink incorporating nanofluid

Rajesh Kumar, R. S. Mishra

Department of Mechanical Engineering, Delhi Technological University, Delhi, India

Article Information

Received: 11 Oct 2022
Revised: 29 Nov 2022
Accepted: 01 Dec 2022
Available online: 31 Dec 2022

Keywords:

Entropy Generation
FOM
Heat Sink
Heat Transfer
Mini-channel
Nanofluids.

Abstract

A 3-D CFD simulation has been used to examine the rate of heat transfer and entropy generation behavior of a circular-shaped mini-channel heat sink. We used Fe_3O_4 /water nanofluid as a coolant and examined the effect of mass flow rate and nanoparticle concentration on cooling potential. The outcome suggests that by increasing the mass flow rate of the coolant, the heat transfer coefficient will be enhanced for both pure water and nanofluid. The nanofluid heat transfer rate will accelerate by raising the concentration of nanoparticles. Results of this analysis show that nanofluid is more efficient than water in the heat sink at any concentration. Characteristics of entropy generation in the heat sink follow a similar pattern to that of the heat transport phenomenon. Entropy generation will be increased by raising the concentration of nanofluid and mass flow rate. Finally, efforts will be made to realize the effective utility of the heat sink in terms of Figures of Merit. By considering FOM (Hav/Sgen), the optimum performance of this present study is achieved at a lower mass flow rate and nanoparticle concentration.

©2022 ijrei.com. All rights reserved

1. Introduction

Research on small heat exchangers has gained significant attention in the last two decades. We are all aware that the enormous heat flux produced by the devices is the main factor in component damage. It is a significant problem for the electronic system to remove heat effectively. A mini-channel heat sink develops a novel cooling technology to remove too much heat from a small space. The mini-channel flow shape provides a strong convective heat transfer coefficient and a large surface area-to-volume ratio. Tuckerman and Pease [1] first proposed the concept of a microchannel heat sink. They conducted tests on a rectangular shape microchannel made up of silicon and demonstrated that this heat sink could significantly lower the surface temperature. Their pioneering

work started another study; many researchers compared their experimental [2-3], numerical [4-5], and analytical [6-7] studies with Tuckerman and Pease. They found that reducing the channel height to micro-scale enhanced the heat transfer compared with conventionally-sized devices. A variety of channel shape, such as circular [8], triangular [9], tapered [10], trapezoidal [11], converging [12], and ribbed [13] has been examined in these studies. It is evident that the channel shape significantly impacts the pressure fall and rate of heat transmission. Many previous evaluation studies have also been devoted to incorporating nanofluids as a coolant rather than pure water. Pak and Cho [14], Hosseini et al. [15], and Li et al. [16] explore the drop in pressure and heat transfer coefficient behavior by the insertion of nanofluid in a heatsink. Their finding suggests that the heat transfer rate is associated with

nanoparticle shape and size, nanofluid concentration, Reynold number, and Nusselt number. Results show that nanofluid is more efficient than water in the heat sink at any concentration. M. Bezaatpour et al. [17] explore a three-dimensional numerical simulation that has been carried out to study the effect of nanofluid on the heat transfer and pressure drop of magnetite nanofluid flow into the heat sink. Ahmet Z. Sahin et al. [18], a numerical solution to the entropy generation in a circular pipe is made.

2. Problem description

Figure 1 indicates the schematic of a compact heat sink made of an aluminium material having a length(L), width(W) of 40 mm, with a height(H) of 10 mm will be simulated. We examine the thermal and hydraulic performance of the device, having a set of similar circular mini channels of the same diameter using either pure water or Fe₃O₄-water nanofluid as coolant. The capability of the heat sink has been studied by keeping laminar flow through the channels for a specific range of variations of different parameters like the coolant's volume flow rate (0.841-3.364 cm³/s) and nanofluid volume fraction (0.01-0.03). Heat flux is uniformly supplied to the bottom wall at the rate of 66 kW/m², while the other surface is insulated.

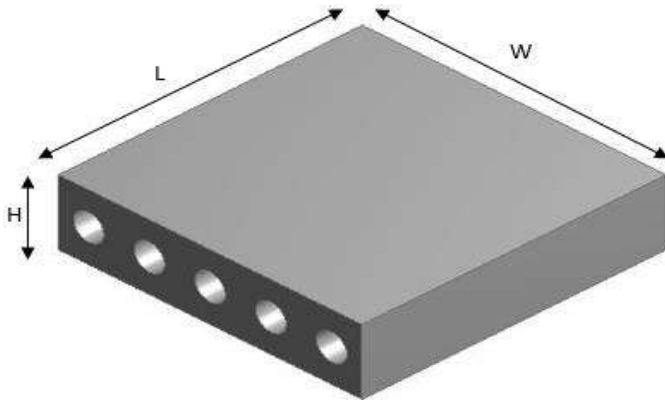


Figure 1: Geometric configuration of the heat sink of diameter 4mm

Table 1: Dimension of the heat sink

W	H	L	n	D
40	10	40	5	4

Table 2: Thermo-physical properties of aluminium [22]

Property	Symbol	Value	Unit
Density	ρ	2787	Kg/m ³
Thermal conductivity	k_s	170	W/m-K
Specific heat	c_p	883	J/kg-K

Table 3: Thermo-physical properties of water at 298K [22]

Property	Symbol	Value	Unit
Density	ρ	996.193	Kg/m ³
Specific heat	c_p	4180	J/kg-K
Thermal conductivity	k_f	0.61195	W/m-K
Dynamic viscosity	μ_f	0.000836	Kg/m-s

Table 4: Properties of nanoparticles [17]

Particle	Diameter(mm)	K(W/m.k)	C _p (J/kg. K)	ρ (kg/m ³)
Fe ₃ O ₄	0.00002	7	640	4950

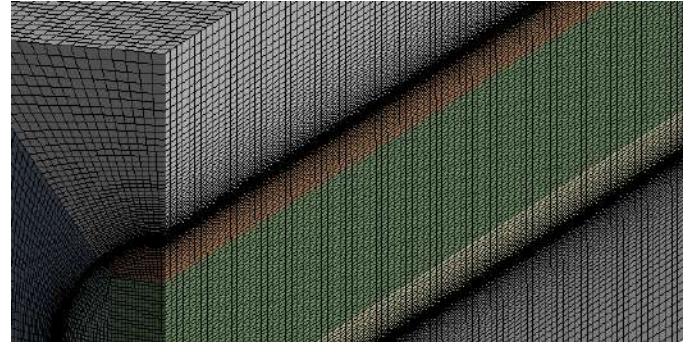


Figure 2: Indicates the grid distribution for fluid and solid regions of the heat sinks.

3. Governing equation and boundary condition

3.1 Governing equations

The ensuing presumption is taken into account a) 3-D flow, b) laminar and incompressible, c) Irrotational flow, d) steady flow, e) Axisymmetric, f) Neglect the body force, g) Thermal radiation is neglected, h) Thermo-physical properties is the function of temperature for nanofluid, but solid properties are taken constant, i) Thermal equilibrium between fluid and solid phase. Under this assumption, the following are the continuity, momentum, and energy governing equations for the fluid and solid domain [19].

3.1.1 Continuity equation

For incompressible flow through the circular channel, the law of conservation of mass in general gives

$$\frac{1}{r} \frac{\partial(ru_r)}{\partial r} + \frac{1}{r} \frac{\partial(u_\theta)}{\partial \theta} + \frac{\partial(u_z)}{\partial z} = 0 \quad (1)$$

3.1.2 Momentum equation

The dominating linear momentum which drives the flow through the channels is the axial component of it, for which the Navier-Stokes equation can be written as

$$\left(u_r \frac{\partial u_z}{\partial r} + \frac{u_\theta}{r} \frac{\partial u_z}{\partial \theta} + u_z \frac{\partial u_z}{\partial z} \right) = -\frac{1}{\rho} \frac{\partial p}{\partial z} + \frac{\mu}{\rho} \left\{ \frac{1}{r} \frac{\partial}{\partial r} \left(r \frac{\partial u_z}{\partial r} \right) + \frac{1}{r^2} \frac{\partial^2 u_z}{\partial \theta^2} + \frac{\partial^2 u_z}{\partial z^2} \right\} \quad (2)$$

The radial and the azimuthal components of the linear momentum equations are expressed, respectively as

$$\left(u_r \frac{\partial u_r}{\partial r} + \frac{u_\theta}{r} \frac{\partial u_r}{\partial \theta} - \frac{u_\theta^2}{r} + u_z \frac{\partial u_r}{\partial z} \right) = -\frac{1}{\rho} \frac{\partial p}{\partial r} + \frac{\mu}{\rho} \left\{ \frac{\partial}{\partial r} \left(\frac{1}{r} \frac{\partial}{\partial r} [ru_r] \right) + \frac{1}{r^2} \frac{\partial^2 u_r}{\partial \theta^2} - \frac{2}{r^2} \frac{\partial u_\theta}{\partial \theta} + \frac{\partial^2 u_r}{\partial z^2} \right\} \quad (3)$$

$$\left(u_r \frac{\partial u_\theta}{\partial r} + \frac{u_\theta}{r} \frac{\partial u_\theta}{\partial \theta} + \frac{u_r u_\theta}{r} + u_z \frac{\partial u_\theta}{\partial z}\right) = -\frac{1}{\rho r} \frac{\partial p}{\partial \theta} + \frac{\mu}{\rho} \left\{ \frac{\partial}{\partial r} \left(\frac{1}{r} \frac{\partial}{\partial r} [r u_\theta] \right) + \frac{1}{r^2} \frac{\partial^2 u_\theta}{\partial \theta^2} + \frac{2}{r^2} \frac{\partial u_\theta}{\partial \theta} + \frac{\partial^2 u_\theta}{\partial z^2} \right\} \quad (4)$$

3.1.3 Equation of energy for coolant

The temperature formulation of the energy equation for fluid flow is framed as follows

$$\rho c_p \left(u_r \frac{\partial T}{\partial r} + \frac{u_\theta}{r} \frac{\partial T}{\partial \theta} + u_z \frac{\partial T}{\partial z}\right) = k_f \left[\frac{1}{r} \frac{\partial}{\partial r} \left(r \frac{\partial T}{\partial r} \right) + \frac{1}{r^2} \frac{\partial^2 T}{\partial \theta^2} + \frac{\partial^2 T}{\partial z^2} \right] + \mu \phi \quad (5)$$

Here, ϕ is the viscous dissipation function and is given by

$$\phi = 2 \left(\frac{\partial u_r}{\partial r} \right)^2 + 2 \left(\frac{1}{r} \frac{\partial u_\theta}{\partial \theta} + \frac{u_r}{r} \right)^2 + 2 \left(\frac{\partial u_z}{\partial z} \right)^2 + \left(\frac{\partial u_\theta}{\partial r} - \frac{u_\theta}{r} + \frac{1}{r} \frac{\partial u_r}{\partial \theta} \right)^2 + \left(\frac{1}{r} \frac{\partial u_z}{\partial \theta} + \frac{\partial u_\theta}{\partial z} \right)^2 + \left(\frac{\partial u_r}{\partial z} + \frac{\partial u_z}{\partial r} \right)^2 \quad (6)$$

3.1.4 Energy equation for the solid region

Assuming that the pure conduction takes place inside the solid domain of the heat sink and no heat source is there inside, the thermal energy equation of solid without any radiation is computed by

$$k_s \left[\frac{1}{r} \frac{\partial}{\partial r} \left(r \frac{\partial T_s}{\partial r} \right) + \frac{1}{r^2} \frac{\partial^2 T_s}{\partial \theta^2} + \frac{\partial^2 T_s}{\partial z^2} \right] = 0 \quad (7)$$

3.2 Thermo-physical properties of nanofluid

The following equation can be used to determine the density, specific heat, and viscosity of nanofluids [17]

$$(\rho)_{nf} = (1 - \phi)\rho + \phi * \rho_{np} \quad (8)$$

$$(\rho * C_p)_{nf} = (1 - \phi)(\rho * C_p)_f + \phi(\rho * C_p)_{np} \quad (9)$$

$$\mu_{nf} = \mu(1 + 2.5\phi) \quad , \phi \leq 2\% \quad (10)$$

$$\mu_{nf} = \frac{\mu_f}{(1-\phi)^{2.5}}, \phi > 2\% \quad (11)$$

Thermal conductivity for nanofluid is evaluated by [17],

$$K_{nf} = K_{static} + K_{brownian} \quad (12)$$

$$K_{static} = K \left[\frac{((K_{np}+2K)-2\phi(K_f-K))}{((K_{np}+2K)+\phi(K_f-K))} \right] \quad (13)$$

$$K_{brownian} = 5 \times 10^4 \beta \phi \rho_f C_{p,f} \sqrt{\frac{k*T}{\rho_{nf}*D_{np}}} \times g(\phi, T) \quad (14)$$

Where $k = 1.3807 \times 10^{-23}$ J/K and β is the fraction of the liquid volume which travels with a particle

$$g = (-6.04\phi + 0.4705)T + 1722.3\phi - 134.69 \quad (15)$$

$$\beta = 0.0017 \times (100 \times \phi)^{(-0.0841)} \quad (16)$$

It is believed that the thermo-physical characteristics of pure water depend on temperature. The consequent model has been utilized to forecast the thermo-physical characteristics of water [17].

$$\rho = 2446 - 20.674T + 0.11576T^2 - 3.12895 \times 10^{-4}T^3 + 4.0505 \times 10^{-7}T^4 - 2.0546 \times 10^{-10}T^5 \quad (17)$$

$$\mu = 2.414 \times 10^{-5} \times 10^{\left(\frac{247.8}{T-140}\right)} \quad (18)$$

$$K = -1.13 + 9.71 \times 10^{-3}T - 1.31 \times 10^{-5}T^2 \quad (19)$$

3.3 Mathematical equations for calculating different parameter

3.3.1 Pressure drop

Pressure drop (Δp) is the difference between inlet and exit pressure when the fluid passes through the pipe. Pressure drop in the pipe from inlet to outlet is computed by:

$$\Delta P = \frac{128\mu QL}{\pi D^4} \quad (20)$$

The loss of energy that occurs when the fluid enters a pipe is called entry loss (Δp_{entry})

$$\Delta P_{entry} = k_{e*} \frac{1}{2} \rho V_{avg}^2 \quad (21)$$

Total pressure drop (ΔP_T):

$$\Delta P_T = \Delta P + \Delta P_{entry} = \frac{128\mu QL}{\pi D^4} + k_{e*} \frac{1}{2} \rho V_{avg}^2 \quad (22)$$

3.3.2 Average heat transfer coefficient

$$h_{ave} = \frac{Q}{A_h \Delta T_m} = \frac{q''}{\Delta T_m} \quad (23)$$

Where A_h is the heat transfer area, q'' is the heat flux ΔT_m is the average temperature difference between the fluid and solid wall.

$$\Delta T_m = T_b - T_f$$

Where

T_b is heat sink base temperature, and T_f is defined as:

$$T_f = \frac{T_{in} + T_{out}}{2}$$

Where, T_{in} and T_{out} are the inlet and outlet fluid temperature, respectively.

3.3.3 Entropy Generation

It measures the quantity of entropy created by any irreversible processes.

Entropy Generation due to Friction

$$(\dot{S}_{gen})_1 = \dot{m} * R * \left(\frac{\Delta P}{P_i}\right) \quad (24)$$

Entropy Generation due to temperature difference

$$(\dot{S}_{gen})_2 = \dot{m} * c_p * \left(\frac{T_e}{T_i}\right) - \left(\frac{Q}{T_w}\right),$$

Where, $\dot{Q} = \dot{q} * \pi * d_h * L$ (25)

$$(\dot{S}_{gen})_{Total} = (\dot{S}_{gen})_1 + (\dot{S}_{gen})_2$$

3.3.4 Pumping power

Pumping power (PP) is the standard for calculating pressure loss between a heat sink's input to output.

$$PP = \Delta p * Q \quad (26)$$

Where, Q is the volume flow rate.

Heat transfer (η) efficiency is defined as:

$$\eta = \frac{h}{h_c} \quad (27)$$

Index c represents a clear channel consisting of pure water as a working fluid.

3.3.5 Figures of merit (FOM)

FOM is the ratio of heat transfer coefficient to entropy generation.

$$FOM = \frac{(h_{av}/s_{gen})_{nf}}{(h_{av}/s_{gen})_w} \quad (28)$$

3.4 Boundary conditions

With a consistent axial velocity determined by the flow rate, the nanofluid enters the channel with a fluid temperature of 298K at the inlet. Initial gauge pressure is fixed to 500 Pa for every analysis, and the nanofluid exit pressure is atmospheric. The heat sink's surface is supposed to be adiabatic irrespective of the bottom surface, at which a consistent heat flux of $66\text{kw}/\text{m}^2$ is applied in all cases. Conditions for no-slip velocity and thermal equilibrium are used at solid-fluid interfaces.

$$u = v = w = 0, T_f = T_s, -k_{nf} \frac{\partial T_f}{\partial n} = -k_s \frac{\partial T_s}{\partial n} \quad (29)$$

4. Numerical modelling, grid independency, and validation of the numerical method

The geometry of the three-dimensional flow domain has been generated using design modular in ANSYS 17.1 as per the physical dimension given in the work of Bezaatpour et al. [17]. Utilizing the finite volume approach, governing equations at specified boundary conditions are resolved. We considered the non-uniform structured grid for the analysis, as shown in figure 2. The grid points are grouped close to the wall due to the high gradient in velocity and temperature. The approach implements for solving the problem is SIMPLE technique (semi-implicit method for pressure-linked equation). The discretization scheme used for pressure, momentum, and energy is presto, second-order upwind, and second-order upwind, respectively, and for gradient LSCB (least squares cell based) method is used. The thresholds for momentum and energy convergence are chosen at 10^{-6} and 10^{-9} , respectively. The result of numerical analysis depends significantly upon the type of meshes and the number of elements therein. Therefore, it must adopt a typical mesh structure and a certain number of elements beyond which numerical simulation results will not vary appreciably. The heat sink's bottom wall temperature was measured using various grid numbers to verify the calculation's correctness and grid independence. The outcomes are compiled in figure 4.1 using various grid numbers.

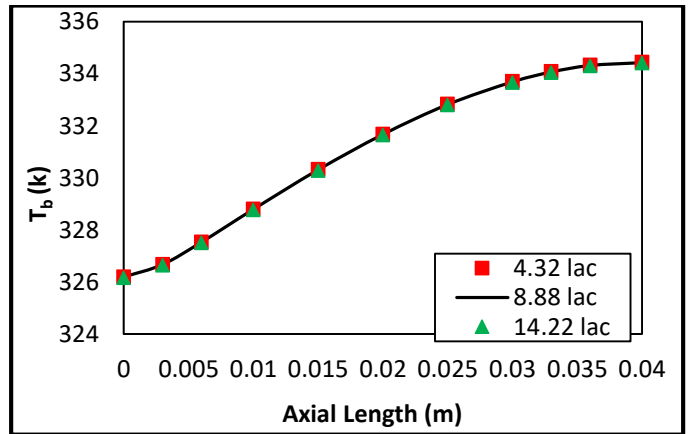


Figure 3: Grid independence test

As understood from Fig. 4.1, the difference between the results obtained from the simulation with a moderate number of elements (around 8-9 lacs) and a more significant number of elements (around 13-14lacs) is quite negligible. Thus around 8-9 lacs of elements have been used for all the simulations.

In order to validate the numerical procedure, a comparison has been made between the current results and the numerical result of Bezaatpour et al. [17] for a mini-channel considering identical geometry, coolant, dimensions, and boundary conditions. Figure 4.2 compares the current numerical result with Bezaatpour et al. [17] result for the variation of heat transfer coefficient with flow rate. The maximum deviation from the experimental results is $< 7\%$, which ensures the preciseness of the present finding.

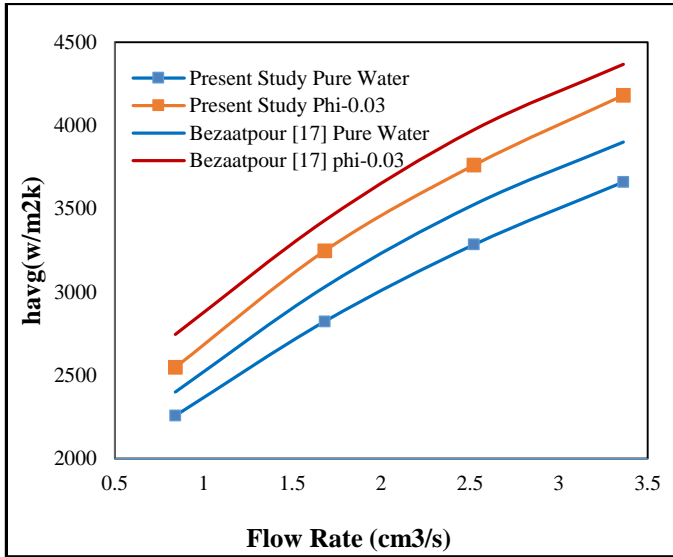


Figure 4: Validation

5. Result and Discussion

5.1 Heat transfer and entropy generation results

To examine the rate of heat transport and entropy generation, coefficient of heat transfers and entropy generation is calculated for each considered condition. We examined its variations with volume flow rate and nanofluid concentration.

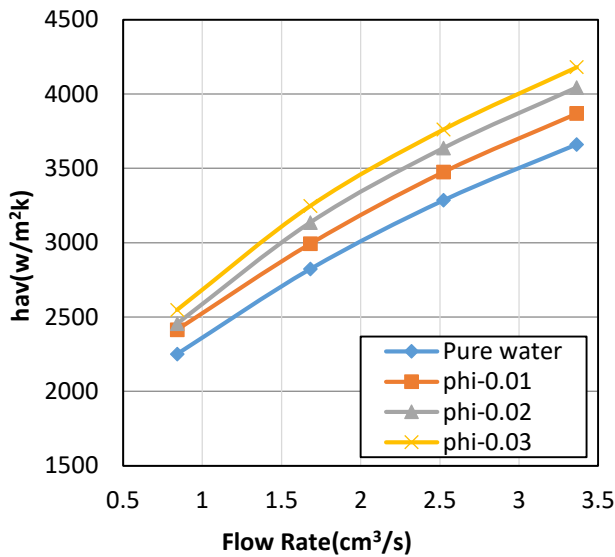


Figure 5: Average heat transfer coefficient variation with flow rate at various nanofluid concentration

According to the abovementioned pattern in figure 5, we have found that increasing the coolant's volume flow rate in the channel will improve the heat transmission rate. Raising the concentration of the nanoparticles in the base fluid will improve heat transfer further. The maximum heat transmission will be achieved at a higher volume flow rate and nanofluid

concentration. From figure 6, it was also found that an increment in the volume flow rate of coolant will enhance the entropy generation of the channel. By introducing nanofluid, the entropy generation will be further enhanced. From the above result it was found that the irreversibility is the function of nanofluid concentration. From figure 7,8, 9, and 10, we found that heat transfer rate and entropy generation is directly associated with Reynolds number as well as Nusselt number. By increasing Reynolds numbers and Nusselt number, both heat transfer and entropy will be increased for water as well as nanofluid.

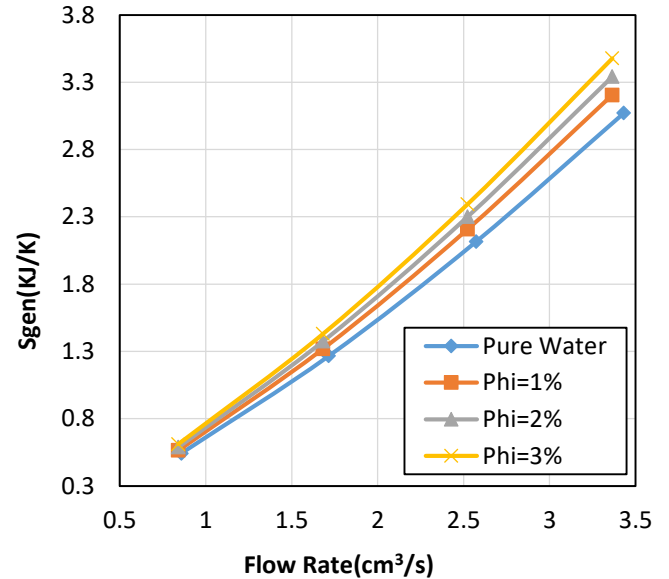


Figure 6: Entropy generation variation with flow rate at various nanofluid concentration

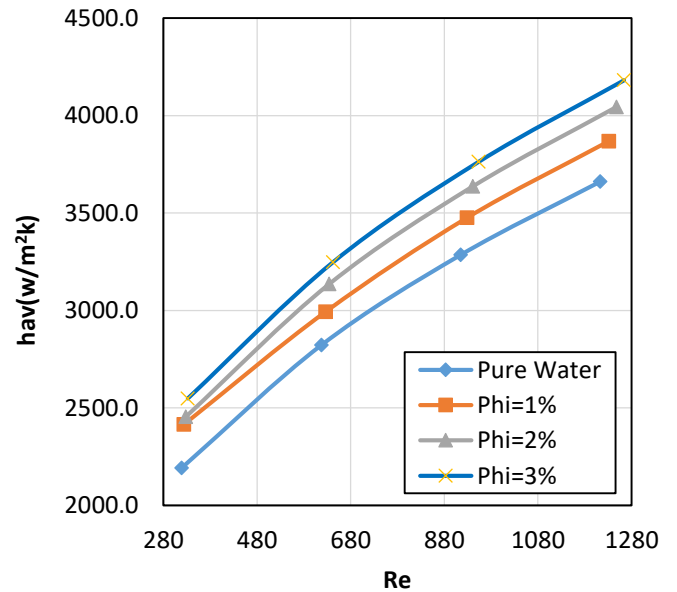


Figure 7: Average heat transfer coefficient variation with Reynold's number at various nanofluid concentration

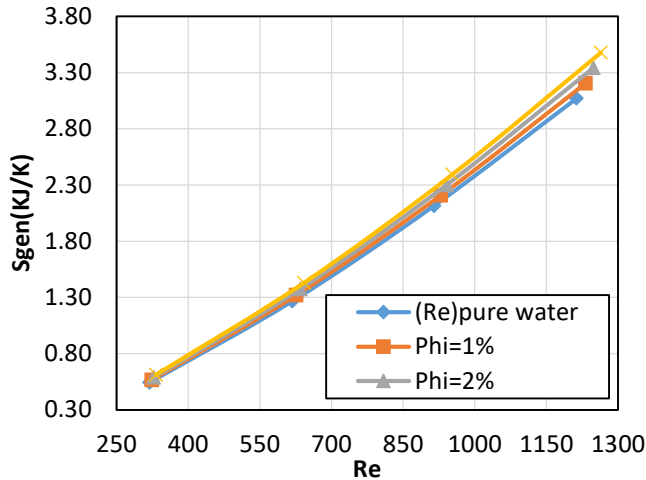


Figure 8: Entropy generation variation with Reynold's number at various nanofluid concentration

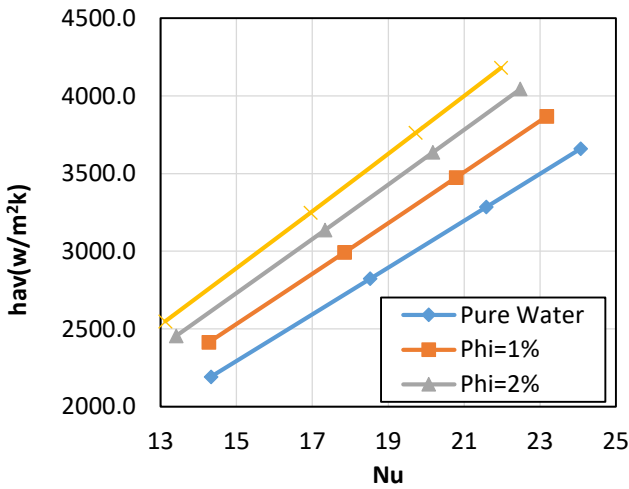


Figure 9: Average heat transfer coefficient variation with Nusselt number at various nanofluid concentration

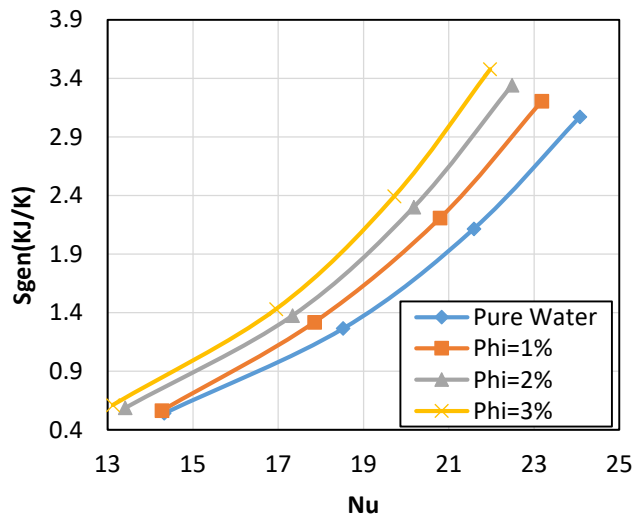


Figure 10: Entropy generation variation with Nusselt number at various nanofluid concentration

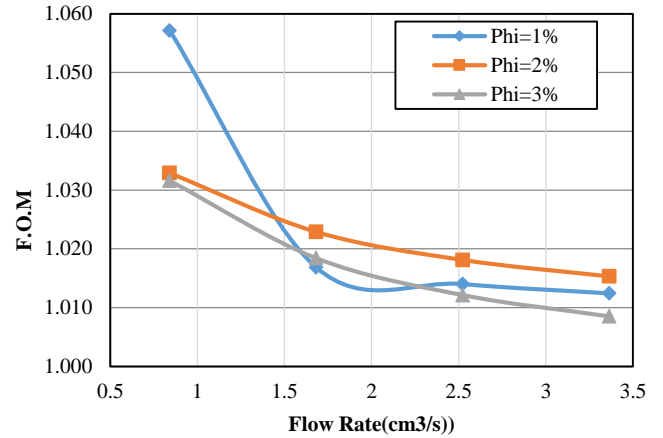


Figure 11: Figure of merit variation with flow rate at various nanofluid concentration

5.2 From a design point of view

We intend to promote the heat transfer rate and minimize the entropy generation of the heat sink. A new parameter is introduced: a figure of merit (H_{av}/S_{gen}). Maximum the value of F.O.M means that the heat transfer corresponding to its entropy generation is maximum. Finally, efforts will be made to realize the effective utility of the heat sink in terms of Figures of Merit. From the above graph, we can find that a lower volume flow rate along with lower nanofluid concentration is the optimal condition for this present study, where we have achieved a satisfactory heat transfer rate for the lower work-loss expense (entropy generation).

6. Conclusions

The consequence of mass flow rate, nanofluid concentration for heat transmission rate, and entropy generation for circular mini-channel heat sink has been examined computationally. The respective outcome has been attained-

- The heat transmission rate is enhanced by increasing the coolant's volume flow rate and the nanofluid's concentration.
- Increasing the Reynolds number and Nusselt numbers will raise the heat transfer for both nanofluids and pure water.
- Increasing nanofluid's volume fraction and flow rate will also increase entropy generation.
- Increasing the volume flow rate will escalate the developing length. A fully developed flow may not be obtained inside the flow domain for a higher volume flow rate.
- F.O.M is decreased by increasing the volume flow rate.
- Maximum heat transfer enhancement achieved by using nanofluid is 13% at phi=0.03.
- Achieving optimum performance of the heat sink by considering FOM, the rigorous performance is achieved at a low volume flow rate and lower nanofluid volume fraction.

Abbreviations

MCHS	Mini-channel heat sink
FOM	Figures of merit
LPM	Litre per minute
PP	Pumping Power
3-D	Three dimensional
CFD	Computational fluid dynamics

Notations

q	Total heating power (W)
q''	Heat flux (W/m^2)
h_{av}	Heat transfer coefficient (W/m^2K)
C_p	Specific heat (KJ/Kg. K)
ΔP	Pressure drop (pa)
S_{gen}	Entropy generation (KJ/K)
f	Frictional factor ($\Delta P D_h / 2L\rho V^2$)
h_x	Local heat transfer coefficient (W/m^2K)
P	Pressure (Pa)
Re	Reynold number
D_h	Hydraulic diameter (m)
Nu	Nusselt number (hD_h/k)
FOM	Figures of merit
Q	Volume flow rate (cm^3/s)
k	Thermal conductivity (W/mK)
V	Velocity (m/s)
T	Temperature

Greek symbols

ϕ	Volume fraction
ρ	Density (kg/m^3)
β	Fraction of liquid volume
η	Heat transfer efficiency
μ	Dynamic viscosity ($N - s/m^2$)

Subscripts

av	Average
in	Inlet
nf	Nanofluid
np	Nanoparticles
s	Solid
w	Wall
b	Bottom wall
i	Initial
f	Final

References

- [1] D.B.Tuckerman, R.F.W. Pease, High-performance heat sinking for VLSI, IEEE Electron Device Lett. 2 (1981) 126-129.
- [2] G.I. Morini, single-phase convective heat transfer in microchannels: a review of experimental results, Int. J. Therm. Sci. 43(2004) 631-651.
- [3] M.M. Rahman, Measurement of heat transfer in microchannel heat sinks, Int. Commun. Heat Mass Transfer. 27(2000) 495-506.
- [4] W. Qu, I. Mudawar, Analysis of three-dimensional heat transfer in microchannel heat sinks, Int. J. Heat Mass Transfer. 45(2002) 3973-3985.
- [5] S.E. Ghasemi, A.A. Ranjbar, M.J.Hosseini, Numerical study on the effect of CuO-water nanofluid on cooling performance of two different cross-sectional heat sinks, Adv. Powder Technology.28(2017) 1495-1504.
- [6] R.W. Knight, J.S. Goodling, D.J.Hall, Optimal thermal design of forced convection heat sinks-analytical, J.Electron. Package. Trans.ASME. 113 (1991) 313-321.
- [7] R.W. Knight, J.S. Goodling, D.J.Hall, R.C.Jaeger, Heat sink optimization with application to microchannels, IEEE Trans. Components hybrids Manuf. Technol. 15(1992) 832-842.
- [8] P. Number, Paper Number ICMM2003-1095 Circular Cooling Microchannels, 2017.
- [9] H.A. Mohammed, P. Gunnasegaran, N.H. Shuaib, The impact of various nanofluid types on triangular microchannels heat sink cooling performance, Int. Commun. Heat Mass Transf. 38 (2011) 767-773.
- [10] T.C. Hung, W.M. Yan, the effect of tapered-channel design on the thermal performance of microchannel heat sink, Int. Commun. Heat Mass Transf. 39 (2012) 1342-1347.
- [11] E. Khodabandeh, A. Abbassi, Performance optimization of water-Al₂O₃ nanofluid flow and heat transfer in a trapezoidal cooling microchannel using constructal theory and two phases Eulerian-Lagrangian approach, Powder Technol. 323 (2018) 103-114.
- [12] M. Dehghan, M. Daneshpour, M.S. Valipour, R. Rafee, S. Saedodin, enhancing heat transfer in microchannel heat sinks using converging flow passages, Energy Convers. Manag. 92 (2015) 244-250.
- [13] L. Chai, G.D. Xia, H.S. Wang, Numerical study of laminar flow and heat transfer in a microchannel heat sink with offset ribs on sidewalls, Appl. Therm. Eng. 92 (2016)32-41.
- [14] B.C. Pak, Y.I. Cho, Hydrodynamic and heat transfer study of dispersed fluids with submicron metallic oxide particles, Exp. Heat Transf. 11 (1998) 151-170.
- [15] S.R. Hosseini, M. Sheikholeslami, M. Ghasemian, D.D. Ganji, Nanofluid heat transfer analysis in a microchannel heat sink (MCHS) under the effect of a magnetic field by means of KKL model, Powder Technol. 324 (2018) 36-47.
- [16] Y. Xuan, Q. Li, Investigation on convective heat transfer and flow features of nanofluids, J. Heat Transf. 125 (2003) 151.
- [17] M. Bezaatpour, M. Gharkhah, Three-dimensional simulation of hydrodynamic and heat transfer the behavior of magnetite nanofluid flow in circular and rectangular channel heat sinks filled with porous media, Powder Technology 344 (2019) 68-78.
- [18] Al-Rashed a, Ranjbarzadeh et al., Entropy generation of boehmite alumina nanofluid flow through a mini-channel heat exchanger considering nanoparticle shape effect, Physica A 521 (2019) 724-736.
- [19] A. Bejan, Convection heat transfer, John Wiley & Sons, Inc, 2013.
- [20] D.A. Nield, A. Bejan, Convection in Porous Media, Springer, 2006.
- [21] A. Bejan, Entropy Generation Minimisation, CRC Press, 1996.
- [22] John H. Lienhard, A Heat Transfer Textbook, Phlosiston Press, 2020.

Cite this article as: Rajesh Kumar, R. S. Mishra, Numerical investigation of thermal performance of heat sink incorporating nanofluid, International Journal of Research in Engineering and Innovation Vol-6, Issue-6 (2022), 399-405.
<https://doi.org/10.36037/IJREI.2022.6605>.